

ChemComm

Accepted Manuscript



This is an *Accepted Manuscript*, which has been through the Royal Society of Chemistry peer review process and has been accepted for publication.

Accepted Manuscripts are published online shortly after acceptance, before technical editing, formatting and proof reading. Using this free service, authors can make their results available to the community, in citable form, before we publish the edited article. We will replace this *Accepted Manuscript* with the edited and formatted *Advance Article* as soon as it is available.

You can find more information about *Accepted Manuscripts* in the [Information for Authors](#).

Please note that technical editing may introduce minor changes to the text and/or graphics, which may alter content. The journal's standard [Terms & Conditions](#) and the [Ethical guidelines](#) still apply. In no event shall the Royal Society of Chemistry be held responsible for any errors or omissions in this *Accepted Manuscript* or any consequences arising from the use of any information it contains.

Cite this: DOI: 10.1039/c0xx00000x

www.rsc.org/xxxxxx

ARTICLE TYPE

Organic Mixed Valency in Quadruple Hydrogen-bonded Triarylamine Dimers Bearing Ureido Pyrimidinedione Moieties[†]

Keishiro Tahara,* Tetsufumi Nakakita, Shohei Katao and Jun-ichi Kikuchi*

Received (in XXX, XXX) Xth XXXXXXXXX 20XX, Accepted Xth XXXXXXXXX 20XX

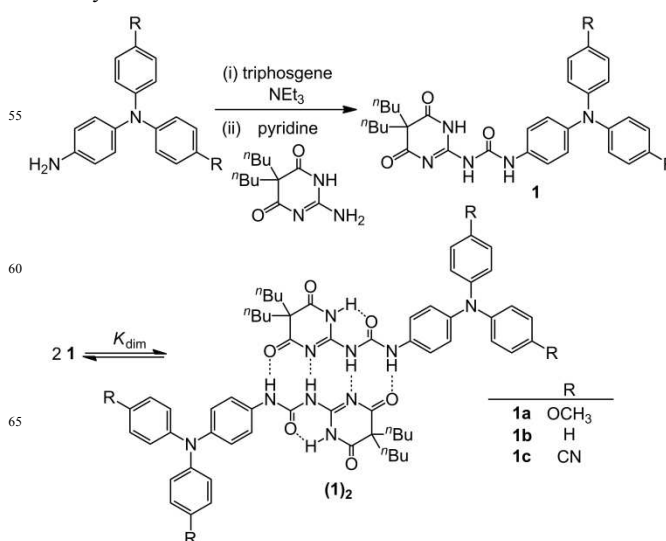
DOI: 10.1039/b000000x

Quadruple hydrogen-bonding interactions stabilized the mixed-valence states of dimers of triarylamine derivatives bearing an ureido pyrimidinedione moiety without any electronic coupling. This study represents the first example of proton-coupled “organic” mixed valency in solution with different substituents being used to control the stability.

Electron transfer (ET) reactions lie at the heart of chemistry and biology. Mixed-valence (MV) compounds provide a platform for basic ET phenomena, relevant to molecular devices,^{1,2} whereas certain biological systems have coupled ET to proton transfer for ATP synthesis.³ The development of models to explore the interface between mixed valency and proton-coupled ET⁴ could provide insights into the effects of hydrogen-bonds (H-bonds) on the stabilization of MV states, charge delocalization and synchronized motion between electrons and protons. Unlike conventional inorganic MV compounds containing two redox-active metal sites linked through coordination bonds,⁵ several inorganic MV systems containing H-bonded bridges^{6–10} have recently been reported in this context. Studies on the dimers of oxo-centred triruthenium clusters linked by carboxylic acids, revealed that the MV states were stabilised by electronic coupling across H-bonds, based on the intervalence charge transfer (IVCT) absorption in the near-infra red (NIR).⁷ Patmore *et al* discovered another stabilization mechanism and named this “proton-coupled mixed valency”,⁹ where coupling was related to the proton coordinate in an H-bonded bridge, with lactam moieties of dimolybdenum complexes to form H-bonded dimers. Despite extensive research, these systems remain poorly understood because of the limited availability of H-bonded MV compounds capable of providing an adequate comparison with their coordinate- or covalently-bonded counterparts.

Triarylamine (NAr₃) are well-known organic redox centres.¹ The advantages of NAr₃ derivatives include the ease with which they participate in one-electron oxidation, the stability of resulting aminium radical cations (NAr₃^{•+}), and the structural variation achievable through N-C cross-coupling reactions.¹¹ MV phenomena associated with the radical cations of bis(triarylamine) bearing π -conjugated bridges have been widely investigated, with a focus on analysing IVCT from one neutral NAr₃ unit to another oxidized NAr₃^{•+} unit.¹² In contrast to inorganic MV systems containing H-bonded bridges, organic counterparts are less well studied,¹³ especially in solution. Here we report the synthesis and characterisation of a series of NAr₃

derivatives capable of quadruple H-bonding (Scheme 1), and report the first example of proton-coupled “organic” mixed valency based on dimeric forms of these derivatives in solution.



Scheme 1. Syntheses and dimerisation of triarylamine derivatives **1**.

Ureido pyrimidinedione (UPy)¹⁴ was selected as an H-bonded bridge for linking organic redox centres because UPy derivatives form stable dimers with large dimerisation constants (K_{dim}) in apolar solutions with various functional units, including aromatic substituents ($K_{dim} = 10^3 \sim 10^5$ in CDCl₃)^{14b} and ferrocene ($K_{dim} > 10^6$ in CDCl₃).⁶ *p*-Substituted NAr₃ derivatives were selected to allow tuning of the organic redox centers.^{11,15} Three target compounds **1** were synthesised bearing different R groups at the *para*-position of the phenyl rings by condensation of the corresponding isocyanates, which were prepared using triphosgene, and the known pyrimidinedione^{14a} (Scheme 1). The yields of **1** increased with the electron-withdrawing strength of the *p*-substituents, which activated the isocyanate starting materials (**1a** 29%; **1b** 36%; **1c** 56%). The new compounds **1a-c** were identified by ¹H- and ¹³C-NMR and ESI-MS (Figs. S1 and S4-9).

In contrast to the pyrimidinedione precursor, compounds **1** were soluble in a range of organic solvents, including chloroform. The ¹H-NMR spectra of **1** in CDCl₃ (**1a** Fig. S4; **1b** Fig. S6; **1c** Fig. S8) contained three NH proton signals that were shifted downfield, indicating involvement in H-bonding. These NH

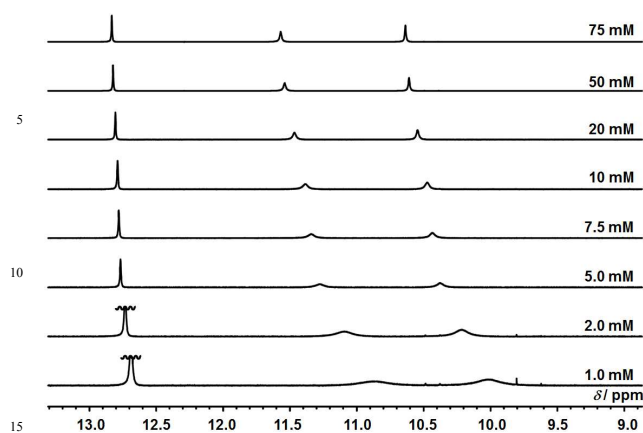


Fig. 1 Partial 600 MHz $^1\text{H-NMR}$ spectra of **1b** at different concentrations in CDCl_3 at 293 K.

proton signals shifted upfield when the concentration of **1** was lowered, as illustrated in the spectra of **1b** obtained at different concentrations (Fig. 1). The lowest field NH proton of **1b** had the smallest shift ($\Delta\delta = 0.134$ ppm in the range of 1.0 to 75 mM) attributed to formation of an intramolecular H-bond, which linearly orientated the DDAA array. The formation of the dimer (**1b**)₂ was confirmed by ESI-mass spectrometry, and **1b** was detected as the monomeric and dimeric Na^+ adducts (Fig. S1). $^1\text{H-NMR}$ binding studies in CDCl_3 at 293 K gave the dimerisation constants. These NMR studies revealed that the K_{dim} values increased with the electron-donating strength of the R groups (**1a** $(6.47 \pm 1.84) \times 10^3$; **1b** $(3.40 \pm 1.64) \times 10^3$; **1c** $(1.51 \pm 0.22) \times 10^3$) (Fig. S14). DFT calculations for the model monomer **1'** bearing ethyl substituents instead of butyl groups (Chart S2) and Mulliken analysis¹⁶ (B3LYP/6-31G(d) levels of theory, Fig. S11 and Tables S3 and S4) revealed that the order of K_{dim} values correlated well with of negative charges on the oxygen atoms of the urea groups (O3 in Chart S2) rather than the corresponding nitrogen atoms (N7 in Chart S2). These results can be understood in terms of the essential pre-organization of the DDAA array into a linear arrangement.

Single crystals of **1a** and **1b** were obtained by recrystallisation from chloroform and hexane, and subjected to X-ray diffraction (XRD) analysis. The molecular structures of **1a** and **1b** are shown in Figs. 2 and S10, respectively. As expected, both compounds existed as dimers, with the individual monomer units connected by DDAA quadruple H-bonds (Table S2). The formation of the dimers (**1**)₂ was also supported by theoretical calculations using a DFT method with the model dimer (**1b'**)₂ (Table S6 and Fig. S12). The optimised geometry of (**1b'**)₂ was similar to that determined for (**1b**)₂ by XRD analysis, with the $\text{N}\cdots\text{O}$ and $\text{N}\cdots\text{N}$ distances of the H-bonds differing by no more than 1.5 pm. The DFT calculations for (**1b'**)₂ also revealed that the highest-lying orbitals (i.e., HOMO and HOMO-1) were localized on the NAr_3 units and not delocalised across the UPy moieties. The calculated HOMO and HOMO-1 of (**1b'**)₂ retained the properties of the isolated monomer **1b'** (Fig. S13). These properties, however, are different from those of the reference compound tetraphenylbenzidine (TPB), which has two chemically equivalent NAr_3 units, where the HOMO was delocalized between the NAr_3 units across a covalent bond.¹⁷

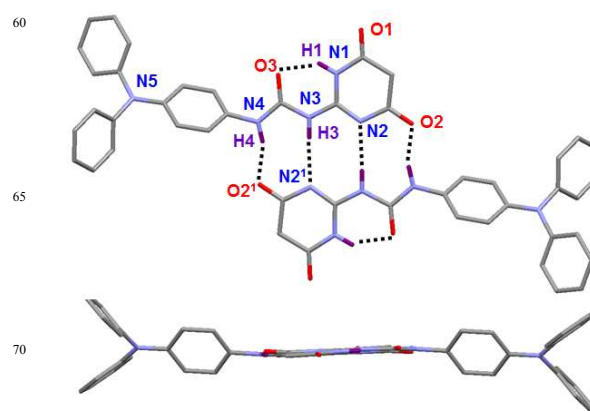


Fig. 2 Crystal structures of **1b**. dotted lines indicate intra- and intermolecular H-bonds; *n*-butyl substituents and hydrogen atoms are omitted for clarity, except for the N-H hydrogens (purple).

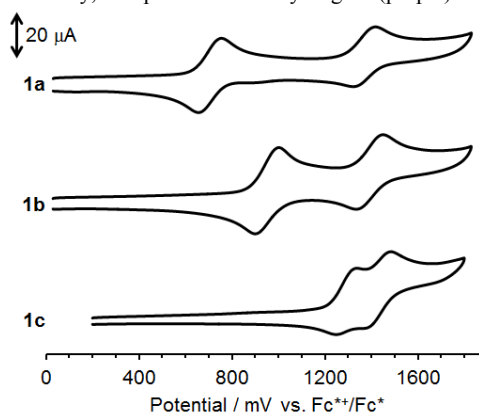


Fig. 3 Cyclic voltammograms of **1** in CH_2Cl_2 containing $n\text{-Bu}_4\text{NPF}_6$ (0.1 M). Scan rate: 100 mV s^{-1} ; $[\mathbf{1}] = 1.0 \text{ mM}$.

Table 1. Electrochemical data for **1**.^a

Cmpd	$E_{1/2}^1$	$E_{1/2}^2$	$\Delta E_{1/2}^b$	K_c^c	σ_p^d
1a	705	1370	665	1.75×10^{11}	-0.27
1b	951	1392	441	2.85×10^7	0
1c	1313	1451	138	211	0.66
TPB	832	1083	251	1.75×10^4	-

^a Potentials in mV vs. Fc^+/Fc^* ($\text{Fc}^* = \text{decamethylferrocene}$). ^b $\Delta E_{1/2}$

^c potential difference between two redox processes.

^d Comproportionation constants obtained from $K_c = \exp(\Delta E_{1/2} F/RT)$.

^e Hammett parameter of the substituents (R) on the phenyl ring.¹⁵

The unique properties of **1** were exemplified by its electrochemical behaviour, which was investigated by cyclic voltammetry (CV) in CH_2Cl_2 containing $n\text{-Bu}_4\text{NPF}_6$ at 298 K. Two well-defined waves were observed for 1.0 mM solutions of **1** (Fig. 3). The first and the second potentials ($E_{1/2}^1$ and $E_{1/2}^2$) are listed in Table 1. The $E_{1/2}^1$ values of **1a-c** decreased as the electron-donating strength of the *p*-substituents increased. This shift in the $E_{1/2}^1$ values for **1** can be understood from the substituent effects and the reference triarylamine derivatives showed similar shifts (Table S7 and Fig. S15). In contrast, the differences in the $E_{1/2}^2$ values were small for compounds **1a-c**, which led to large differences in their potential splitting values $\Delta E_{1/2} (= E_{1/2}^2 - E_{1/2}^1)$. The unique electrochemical behaviour of **1** could be attributed to the sequential oxidation of the two NAr_3 units in the dimeric form (**1**)₂ to give the one- and two-electron-

oxidized species, $(\mathbf{1})_2^+$ and $(\mathbf{1})_2^{2+}$, respectively (eq. 1). Similar redox splitting and stabilization behaviours have also been reported for other MV species, including a H-bonded ferrocenyl dimer containing the same UPy unit as $\mathbf{1}$,⁶ and other inorganic H-bonded dimers.⁷⁻⁹ Two well-defined reversible waves were also observed for **TPB**, which is a covalent analogue. This indicates that the two NAr_3 units underwent sequential oxidation to form one- and two-electron-oxidized species, $\text{TPB}^{+\cdot}$ and TPB^{2+} , respectively.^{1,17} The MV species $\text{TPB}^{+\cdot}$ was stabilized by through-bond electronic interactions (Fig. S13), whereas the MV species $(\mathbf{1})_2^+$ was likely stabilized by a different mechanism. The through-space electrostatic interactions between the NAr_3 units in $(\mathbf{1})_2$ could not account for the relatively large thermodynamic stability for $(\mathbf{1})_2^+$ because of the long $\text{N}\cdots\text{N}$ distances (e.g., 18.596 Å for $(\mathbf{1b})_2$ by XRD analysis).

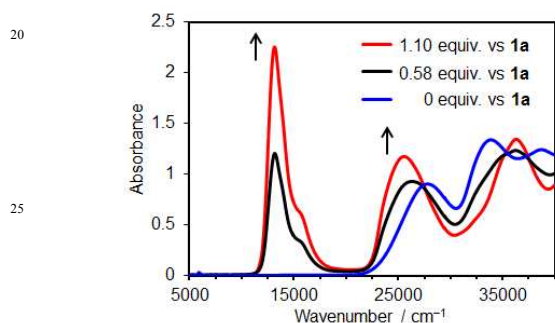
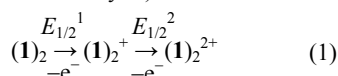


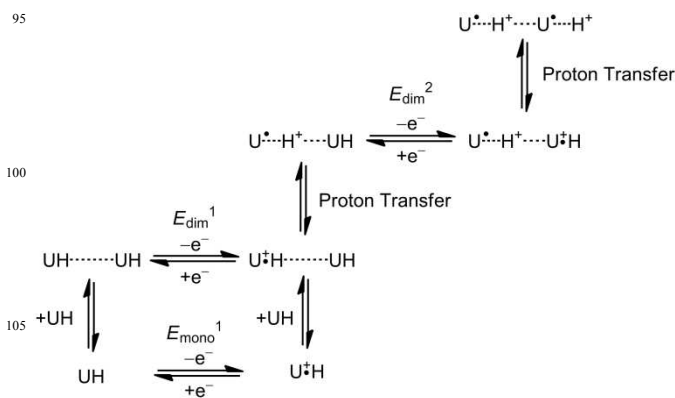
Fig. 4 UV-vis-NIR spectra of $\mathbf{1a}$ (5.0×10^{-4} M) in CH_2Cl_2 in the absence and presence of AgSbF_6 at 298K.

To understand the mechanisms involved in stabilization of the MV state, the dimeric species $(\mathbf{1})_2$ was subjected to chemical oxidation in CH_2Cl_2 with AgSbF_6 (0.65 V vs. Fc^+/Fc in $\text{CH}_2\text{Cl}_2/n\text{-Bu}_4\text{NPF}_6$ ¹⁸; see the potential data for $\mathbf{1}$ quoted relative to the Fc^+/Fc couple in Table S8). Oxidation of $(\mathbf{1})_2$ using 0.58 equiv. of AgSbF_6 with respect to $\mathbf{1a}$ resulted in the formation of a new strong absorption band at 761 nm, which was associated with the $\pi\text{-}\pi^*$ transition of the $\text{NAr}_3^{+\cdot}$ moiety (Fig. 4). The detection of the $(\mathbf{1a})_2^+$ species in the reaction solution by ESI-MS suggested that the dimeric structure was likely maintained (Fig. S21), which is consistent with the DFT calculation as discussed below. There was a 2-fold increase in the absorption intensity when AgSbF_6 was increased to 1.10 equiv. with respect to $\mathbf{1a}$. Further increases of AgSbF_6 , however, had no impact on the absorption intensity, which indicated that the NAr_3 units present in the solution were fully oxidized to the corresponding $\text{NAr}_3^{+\cdot}$ species ($\epsilon_{761} \sim 4.5 \times 10^4 \text{ cm}^{-1}\text{M}^{-1}$). It is noteworthy that an IVCT band was not observed in the NIR region during the oxidation process.¹⁹ The formation of a $\pi\text{-}\pi^*$ transition band and the lack of an IVCT band was also confirmed using another oxidizing agent, SnCl_5 ,²⁰ in a homogeneous CH_2Cl_2 solution system, as shown in Fig. S18.

The lack of electronic coupling between the NAr_3 and $\text{NAr}_3^{+\cdot}$ units in the MV species $(\mathbf{1a})_2^+$ was unambiguously confirmed by a spectroelectrochemical method. When the electrolysis of a solution of $\mathbf{1a}$ was carried out at $E_{\text{ox}}^1 (= E_{1/2}^1 + 0051 \text{ V})$ in $\text{CH}_2\text{Cl}_2/n\text{-Bu}_4\text{NPF}_6$, the absorption intensity of the

$\pi\text{-}\pi^*$ transition of the $\text{NAr}_3^{+\cdot}$ moiety at 760 nm was roughly half of that obtained for $\mathbf{1a}^+$ using the chemical oxidation process described above (Fig. S16). This result indicated that only half of the NAr_3 units were oxidized, which was consistent with the potential splitting observed electrochemically. In accordance with the chemical oxidation results, the $(\mathbf{1})_2^+$ species did not exhibit any IVCT bands in the NIR region spectroelectrochemically. This result was contrary to that reported for a corresponding covalent species 4,4'-{bis[*N,N*-di(4-methoxyphenyl)amino]phenylethynyl}benzene, which had a large $\text{N}\cdots\text{N}$ distance of 19.30 Å but retained an electronic coupling integral of 500 cm^{-1} in its radical cation form.¹⁷

The chemical oxidation of $(\mathbf{1b})_2$ with AgSbF_6 required a longer reaction time for completion and a larger amount of oxidant than that required for the oxidation of $(\mathbf{1a})_2$, as shown in Fig. S19a. The differences in reactivity of dimers reflected the differences in their $E_{1/2}^1$ values. The stepwise addition of AgSbF_6 (until 1.0 equiv. with respect to $\mathbf{1b}$) to a solution of $(\mathbf{1b})_2$ confirmed that the absorption around 750 nm was caused by the $\text{NAr}_3^{+\cdot}$ moiety, and that the lack of an IVCT band. In the presence of excess AgSbF_6 , a new NIR band formed around 1500 nm, and became more intense with time (Fig. S19b). Based on similarities between this new peak and an IVCT band reported in the literature for $\text{TPB}^{+\cdot}$,²¹ the NIR band observed in this study was assigned to the IVCT transition of a $\text{TPB}^{+\cdot}$ derivative rather than that of $(\mathbf{1b})_2^+$. This $\text{TPB}^{+\cdot}$ derivative was likely formed from a radical-radical coupling reaction of $\mathbf{1b}^+$ followed by deprotonation and oxidation of the resulting **TPB** derivative by an excess of AgSbF_6 (Scheme S1). Indeed, the $\text{TPB}^{+\cdot}$ derivative was detected by MALDI-TOF-MS in the reaction of $\mathbf{1b}$ with another chemical oxidant, $\text{Cu}(\text{ClO}_4)_2$ (Fig. S22). The UV-vis-NIR spectral change in the reaction was essentially the same as that with AgSbF_6 . The reactivity of $\mathbf{1b}$ is consistent with a previous report on those of NAr_3 derivatives.²¹ These results indicate that the chemical oxidation of $\mathbf{1b}$ were different to that of the electrochemical oxidation on a typical CV time scale.²²



Scheme. 2 Possible mechanism for the electrochemical reaction of $\mathbf{1}$ (UH).

These results rule out the possibility of electronic interactions between the NAr_3 units in $(\mathbf{1})_2$ stabilizing the MV state. Proton-coupled MV is therefore the most likely mechanism for the stabilization of $(\mathbf{1})_2^+$. A possible mechanism for the electrochemical behaviour of $\mathbf{1}$ is shown in Scheme 2 where the redox-active urea monomers $\mathbf{1}$ are expressed as UH. Although the

UH monomers are in equilibrium with the corresponding dimers UH...UH, the oxidation potentials for UH and UH...UH (i.e., E_{mono}^1 and E_{dim}^1 , respectively) are distributed around the $E_{1/2}^1$ values shown in Table 1. This is reasonable because the difference between the HOMO levels of **1b'** and (**1b'**)₂ are relatively small (Fig. S13).²³ DFT calculations revealed that the one-electron-oxidized species **1**⁺⁺ retained the linear orientation of the DDAA arrays through the intramolecular H-bonds (Fig. S11 and Tables S3 and S5). In addition, increased positive charges on the NH hydrogen atom of **1**⁺⁺ (H17 in Chart S2) compared to those of **1b'** are advantageous for forming intermolecular H-bonds (Table S4). Thus, the MV U⁺⁺H...UH species form from UH...UH by one-electron oxidation, and from UH, which binds more strongly to UH⁺⁺ than itself. This is consistent with a previous report on electrochemically controlled H-bonding using a redox-active urea.²⁴ Following the formation of the MV U⁺⁺H...UH species, the coordinate of the H-bonding proton in the oxidized U⁺⁺H shifts to the neutral UH site because of the enhanced acidity from the one-electron oxidation process. This proton-transfer process increases the oxidation potentials of other neutral NAr₃ moieties in the H-bonded dimers to give the $E_{1/2}^2$ values shown in Table 1, and results in the stabilization of (**1**)₂⁺. Although changes in the scan rate changed the shape of the redox waves and anodic-cathodic peak separation properties for (**1**)₂ (Fig. S17), this effect was minor because of the short-range proton-transfer in (**1**)₂⁺ inside the apolar solvent cage. Following their pioneering work involving H-bonded biimidazolate rhenium dimers, Tadokoro *et al.*⁸ also concluded that the MV state was stabilized by proton-transfer between the complementary H-bond moieties, without participation of solvent molecules.

In summary, three triarylamine derivatives **1a-c** were synthesised and formed dimers (**1**)₂ in the solid state and solution through quadruple H-bonds. Electrochemical and mechanistic investigations revealed the formation of an MV species (**1**)₂⁺, which had no electronic coupling between the NAr₃ and NAr₃⁺⁺ moieties. This study represents the first reported example of proton-coupled “organic” mixed valency in solution with different substituents being used to control the stability.

This work was supported in part by a Grant-in-Aid for Young Scientists B (No. 25790016) and a research grant from the Murata Science Foundation. The authors would like to thank Mr Fumio Asanoma and Ms Yoshiko Nishikawa (NAIST) for their assistance with the NMR and ESI-MS measurements, respectively.

Notes and references

^a Graduate School of Materials Science, Nara Institute of Science and Technology (NAIST), 8916-5, Takayama, Ikoma, Nara 6300192, Japan.

† Electronic Supplementary Information (ESI) available: Experimental details for synthesis, characterisation, XRD analysis and DFT calculation of **1** and related compounds. See DOI:10.1039/b000000x/

- (a) J. Hankache and O. S. Wenger, *Chem. Rev.*, 2011, **111**, 5138-5178. (b) A. Heckmann and C. Lambert, *Angew. Chem. Int. Ed.*, 2012, **51**, 326-292.
- (a) B. He and O. S. Wenger, *J. Am. Chem. Soc.*, 2011, **133**, 17027-17036. (b) O. S. Wenger, *Chem. Soc. Rev.*, 2012, **41**, 3772-3779.
- R. J. P. Williams, *Nature*, 1995, **376**, 643.

- (a) M. H. V. Huynh and T. J. Meyer, *Chem. Rev.*, 2007, **107**, 5004-5064. (b) C. Costentin, M. Robert and J.-M. Saveant, *Chem. Rev.*, 2010, **110**, PR1-PR40.
- For selected reviews, see: (a) K. D. Demadis, C. M. Hartshorn, and T. J. Meyer, *Chem. Rev.*, 2001, **101**, 2655-2685. (b) B. S. Brunschwig, C. Creutz and N. Suih, *Chem. Soc. Rev.*, 2002, **31**, 168-184. (c) W. Kaim and B. Sarkar, *Coord. Chem. Rev.*, 2007, **251**, 584-594.
- H. Sun, J. Steeb and A. E. Kaifer, *J. Am. Chem. Soc.*, 2006, **128**, 2820-2821.
- (a) J. C. Goeltz and C. P. Kubiak, *J. Am. Chem. Soc.*, 2010, **132**, 17390-17392. (b) G. Canzi, J. C. Goeltz, J. S. Henderson, R. E. Park, C. Maruggi and C. P. Kubiak, *J. Am. Chem. Soc.*, 2014, **136**, 1710-1713.
- M. Tadokoro, T. Inoue, S. Tamaki, K. Fujii, K. Isogai, H. Nakazawa, S. Takeda, K. Isobe, N. Koga, A. Ichimura and K. Nakasuji, *Angew. Chem. Int. Ed.*, 2007, **46**, 5938-5942.
- (a) L. A. Wilkinson, L. McNeill, A. J. H. M. Meijer and N. J. Patmore, *J. Am. Chem. Soc.*, 2013, **135**, 1723-1726. (b) L. A. Wilkinson, L. McNeill, P. A. Scattergood and N. J. Patmore, *Inorg. Chem.*, 2013, **52**, 9683-9691.
- M. Pichlmaier, R. F. Winter, M. Zabel and S. Zališ, *J. Am. Chem. Soc.*, 2009, **131**, 4892-4903.
- T. P. Bender, J. F. Graham and J. M. Duff, *Chem. Mater.*, 2001, **13**, 4105-4111.
- (a) A. Heckmann, S. Amthor and C. Lambert, *Chem. Commun.*, 2006, 2959-2961. (b) S. Barlow, C. Risko, S. A. Odum, S. Zheng, V. Coropceanu, L. Beverina, J.-L. Brédas and S. R. Marder, *J. Am. Chem. Soc.*, 2012, **134**, 10146-10155.
- (a) T. Isono, H. Kamo, A. Ueda, K. Takahashi, A. Nakao, R. Kumai, H. Nakao, K. Kobayashi, Y. Murakami and H. Mori, *Nat. Commun.*, 2013, **4**, 1344-1349. (b) S. C. Lee, A. Ueda, H. Kamo, K. Takahashi, M. Uruichi, K. Yamamoto, K. Yakushi, A. Nakao, R. Kumai, K. Kobayashi, H. Nakao, Y. Murakami and H. Mori, *Chem. Commun.*, 2012, **48**, 2959-2961.
- (a) P. K. Baruah, R. Gonnade, U. D. Phalgune and G. J. Sanjayan, *J. Org. Chem.*, 2005, **70**, 6461-6467. (b) L. Cui, S. Gadde, A. D. Shukla, H. Sun, J. T. Mague and A. E. Kaifer, *Chem. Commun.*, 2008, 1446-1448.
- C. Hansh, A. Leo and R. W. Taft, *Chem. Rev.*, 1991, **91**, 165-195.
- R. S. Mulliken, *J. Chem. Phys.*, 1935, **3**, 573-585.
- C. Lambert and G. J. Nöll, *J. Am. Chem. Soc.*, 1999, **121**, 8434-8442.
- (a) N. G. Connelly and W. E. Geiger, *Chem. Rev.*, 1996, **86**, 877-910. (b) L. Song and W. C. Troglor, *Angew. Chem. Int. Ed. Engl.*, 1992, **31**, 770-772.
- The lack of an IVCT band was also confirmed using AgSbF₆ in another non-protic solvent, 1,2-dichloroethane, as shown in Fig. S20. $E_{1/2}^1 = 695$, $E_{1/2}^2 = 1354$ mV vs. Fc^{+/0} and $\Delta E_{1/2} = 659$ mV in the solvent.
- H. Murata and P. M. Lahti, *J. Org. Chem.*, 2007, **72**, 4974-4977.
- K. Sreenath, C. V. Suneesh, V. K. R. Kumar and K. R. Gopidas, *J. Org. Chem.* 2008, **73**, 3245-3251.
- The chemical oxidation of (**1c**)₂ was not investigated in this study because it was expected that the oxidized species would be difficult to form based on the relatively high $E_{1/2}^1$ value.
- Indeed, the electrochemical response for [**1**] = 10 mM was analogous to that of [**1**] = 1.0 mM, with the concentration having very little influence on the shape of the voltammogram.
- J. E. Woods, Y. Ge and D. K. Smith, *J. Am. Chem. Soc.*, 2008, **130**, 1070-1071.